

Article

Immobilization of Potassium-Based Heterogeneous Catalyst over Alumina Beads and Powder Support in the Transesterification of Waste Cooking Oil

Muhammad Amirrul Hakim Lokman NollHakim ^{1,*}, Norshahidatul Akmar Mohd Shohaimi ^{1,*},
Wan Nur Aini Wan Mokhtar ², Mohd Lokman Ibrahim ^{3,4} and Rose Fadzilah Abdullah ⁵

¹ Kampus Jengka, Faculty of Applied Sciences, Universiti Teknologi MARA Cawangan Pahang, Bandar Tun Abdul Razak 26400, Malaysia; amirrul.muhammad@gmail.com

² Department of Chemical Sciences, Faculty of Science and Technology, Universiti Kebangsaan Malaysia (UKM), Bangi 43600, Malaysia; wannurainiwm@ukm.edu.my

³ School of Chemistry and Environment, Faculty of Applied Sciences, Universiti Teknologi MARA, Shah Alam 40450, Malaysia; mohd_lokman@uitm.edu.my

⁴ Centre for Functional Materials and Nanotechnology, Institute of Science, Universiti Teknologi MARA, Shah Alam 40450, Malaysia

⁵ Institute of Advance Technology, Universiti Putra Malaysia (UPM), Serdang 43400, Malaysia; rosa_476@yahoo.com

* Correspondence: akmarshohaimi@uitm.edu.my; Tel.: +609-460-2644



Citation: Lokman NollHakim, M.A.H.; Shohaimi, N.A.M.; Mokhtar, W.N.A.W.; Ibrahim, M.L.; Abdullah, R.F. Immobilization of Potassium-Based Heterogeneous Catalyst over Alumina Beads and Powder Support in the Transesterification of Waste Cooking Oil. *Catalysts* **2021**, *11*, 976. <https://doi.org/10.3390/catal11080976>

Academic Editor: Diego Luna

Received: 27 June 2021

Accepted: 10 August 2021

Published: 15 August 2021

Publisher's Note: MDPI stays neutral with regard to jurisdictional claims in published maps and institutional affiliations.



Copyright: © 2021 by the authors. Licensee MDPI, Basel, Switzerland. This article is an open access article distributed under the terms and conditions of the Creative Commons Attribution (CC BY) license (<https://creativecommons.org/licenses/by/4.0/>).

Abstract: In this work, the beads and powder potassium hydroxide (KOH) and potassium carbonate (K_2CO_3) supported on alumina oxide (Al_2O_3) were successfully prepared via incipient wetness impregnation technique. Herein, the perforated hydrophilic materials (PHM) made from low-density polyethylene (LDPE) was used as the catalyst reactor bed. The prepared catalysts were investigated using TGA, XRD, BET, SEM-EDX, TPD, FTIR while spent catalysts were analyzed using XRF and ICP-AES to study its deactivation mechanism. The catalytic performance of beads and powder KOH/Al_2O_3 and K_2CO_3/Al_2O_3 catalysts were evaluated via transesterification of waste cooking oil (WCO) to biodiesel. It was found that the optimum conditions for transesterification reaction were 1:12 of oil-to-methanol molar ratio and 5 wt.% of catalyst at 65 °C. As a result, the mesoporous size of beads KOH/Al_2O_3 and K_2CO_3/Al_2O_3 catalysts yielded 86.8% and 77.3% at 2 h' reaction time of fatty acids methyl ester (FAME), respectively. It was revealed that the utilization of PHM for beads K_2CO_3/Al_2O_3 increase the reusability of the catalyst up to 7 cycles. Furthermore, the FAME produced was confirmed by the gas chromatography-mass spectroscopic technique. From this finding, beads KOH/Al_2O_3 and K_2CO_3/Al_2O_3 catalysts showed a promising performance to convert WCO to FAME or known as biodiesel.

Keywords: biodiesel; waste cooking oil; transesterification; K_2CO_3/Al_2O_3 ; KOH/Al_2O_3

1. Introduction

One of the most promising and safest means to overcome the global environmental issue is by replacing conventional diesel with biodiesel generated from edible and non-edible plant oils or animal fats [1,2]. Theoretically, biodiesel has low sulfur content than petrol diesel and could reduce hazardous gas emissions, such as SO_2 , NO_2 , CO_2 , and particulate matter, generally produced by diesel engines [3]. Nowadays, scientists believed that the utilization of WCO as the biodiesel feedstock could reduce environmental pollutions.

Esterification and transesterification processes are the common techniques to produce biodiesel. Both techniques generally assist by heterogeneous or homogeneous catalyst either acidic or basic. The homogeneous catalytic reaction is defined as the catalyst that has the same phase as a solvent and is found to have several drawbacks, such as (i) corrosion of container pipelines [4], (ii) wastewater pollutions, and (iii) weak catalyst

recovery [5]. The heterogeneous catalyst was introduced because of easy preparation, affordability and promising high biodiesel conversion. The chemical characteristic of the catalyst can be acidic or basic depending on the method used. Example of acid catalysts used are such as sulfonated D-glucose [6], MF-SO₃H [7], and SiO₂(CH₂)₃NHSO₃H [8]; while, for basic catalyst used such as KOH/NaY [9], Ca/Ba/Al₂O₃ [10], MgO/Al₂O₃ [11], and K₃PO₄/Ac [12]. The chemical characteristic of the catalyst is important to know to match with the feedstock used.

Recently, the powdered heterogeneous catalysts such as RHC/K₂O/Fe [13] and KOH/Al₂O₃ [14] have been utilized in conversion of biodiesel from WCO. However, the powder catalyst has drawbacks such as easy deactivation of catalyst upon exposure to the reaction medium [15], incompatibility with the large batch of the reactor [16], and weak catalyst recovery that leads to difficulties in recycling the catalyst [17]. The use of heterogeneous beads catalysts has been considered. The beads catalyst has an advantage in terms of its different geometrical shapes that create various pores, allowing the optimum hydrodynamic and contact between reactant, catalyst, and solvent to increasing the catalyst's performance [18].

Several heterogeneous beads catalysts are reported compatible with biodiesel production [19,20], such as K₂CO₃/Al₂O₃ and KOH/Al₂O₃ due to their simple preparation, low cost, and high-yield capacity of biodiesel production [21,22]. The reversible chemisorption on both K₂CO₃/Al₂O₃ and KOH/Al₂O₃ was reported to be stable at higher temperature and pressure [23–25], making the essential salt suitable as a catalyst for the reactions. The alkaline-catalyzed transesterification process is generally adopted for biodiesel production because alkaline metal alkoxides and hydroxides are the most effective transesterification catalysts compared to the acid catalysts. However, for economic reasons, hydroxides are more often used.

This research aims to improve and study the binding strength between K₂CO₃ and KOH onto Al₂O₃ beads support and Al₂O₃ powder with a simple, environmental-friendly, and green preparation technique by using perforated hydrophilic material (PHM) as reactor container for beads catalyst. To the best of our knowledge, this is the first reported paper to discuss the utilization of PHM reactor for the protection and stability of the catalyst. This study also focused on the effect of alumina beads-supported K₂CO₃ and KOH catalysts on the transesterification of WCO with low free fatty acid (FFA) numbers. Besides, the PHM reactor made from low-density polyethylene (LDPE) for reactor container was introduced to reduce the catalyst damage and deactivation due to physical contact with the stirrer. The PHM reactor was designed as a porous catalyst container that helps the catalyst maintain its shape before and after the reaction. The solution can easily pass through the container via a tiny hole. The effects of the catalyst preparation, reaction conditions, catalyst performance, and catalyst reusability, were also investigated and discussed in this paper.

2. Results and Discussion

2.1. Thermogravimetric Analysis

In this work, to determine the optimum calcination temperature for the catalyst, the thermal gravimetric analysis (TGA) was carried out; thus, both powdered and beads K₂CO₃/Al₂O₃ and KOH/Al₂O₃ catalysts were analyzed. As shown in Figure 1, results of all prepared catalysts ranging between 32 and 1000 °C showed four stages of decomposition phase, which are: (1) Evaporation of water molecules for all catalyst in between 32 °C and 100 °C [14,26]; (2) commencement of dehydroxylation of OH⁻ molecules [27]; and (3) observation of broadband of K₂CO₃/Al₂O₃ catalyst, indicating the decomposition of KHCO₃ [28].

At stage 3, the 25% decomposition of KAl(CO₃)(OH)₂ occurred for beads K₂CO₃/Al₂O₃ ranging from 300 to 400 °C [29]. While the last decomposition phase at stage 4, represents the successful activation of the catalyst as a result of the formation of K₂O and K₂O₂ has been reported in XRD (Figure 2). The optimum calcination temperature of 700 °C was chosen based on the average of 850 °C and 650 °C, the temperatures at which for both

powder and beads Al_2O_3 treated with KOH showed the formation of K_2O_2 ($4\text{KOH} + \text{O}_2 \rightarrow 2\text{K}_2\text{O}_2 + 2\text{H}_2\text{O}$) and additional active species for K_2CO_3 showed the formation of K_2O ($2\text{K}_2\text{CO}_3 + \text{O}_2 \rightarrow 2\text{CO}_2 + \text{O}_2 + \text{K}_2\text{O}$) species on the Al_2O_3 [18]. For the $\text{K}_2\text{CO}_3/\text{Al}_2\text{O}_3$ powder catalyst (Figure 1c), the desorption peak is very small because the layer is compressed in one thermogram. The effect of decomposition rate between powder and beads catalyst is not much different, so the decomposition of $\text{K}_2\text{CO}_3/\text{Al}_2\text{O}_3$ powder catalyst can be referred to $\text{K}_2\text{CO}_3/\text{Al}_2\text{O}_3$ beads catalyst. A study from Sharikh et al. [30] also stated that by using K_2CO_3 catalyst, the suitable calcination temperature was at 700°C because of the activation of the catalyst in the range of 680°C to 1000°C . Meanwhile, starting from 700°C , the powder and beads Al_2O_3 treated with K_2CO_3 showed the formation of K_2O with the simultaneous loss of carbon dioxide [31]. The catalyst studied showed good strength and stability at high temperatures making the hydrophobic characteristic of the catalyst more efficient toward biodiesel production.

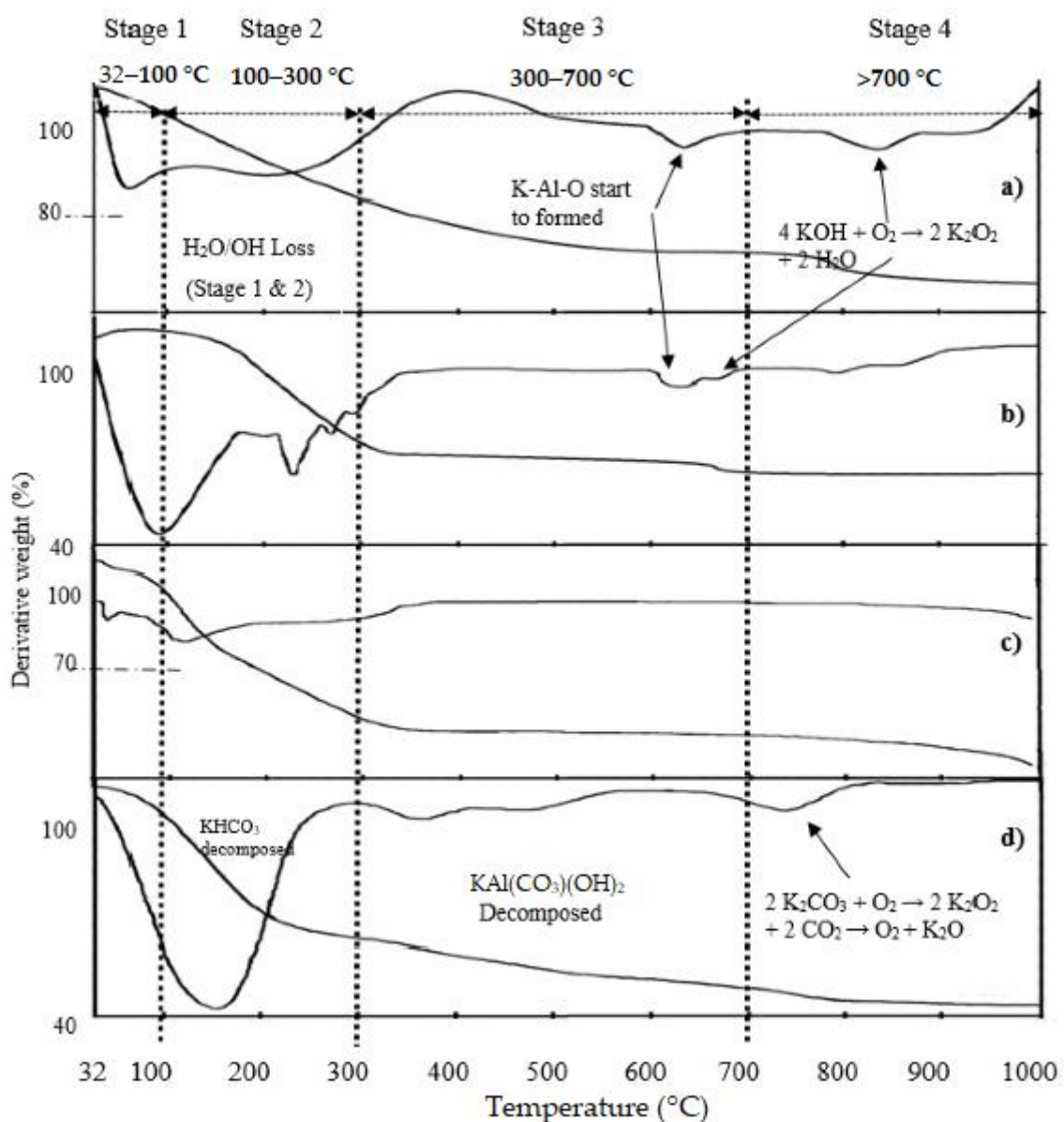


Figure 1. TGA thermogram of (a) powder $\text{KOH}/\text{Al}_2\text{O}_3$, (b) beads $\text{KOH}/\text{Al}_2\text{O}_3$, (c) powder $\text{K}_2\text{CO}_3/\text{Al}_2\text{O}_3$, and (d) beads $\text{K}_2\text{CO}_3/\text{Al}_2\text{O}_3$.

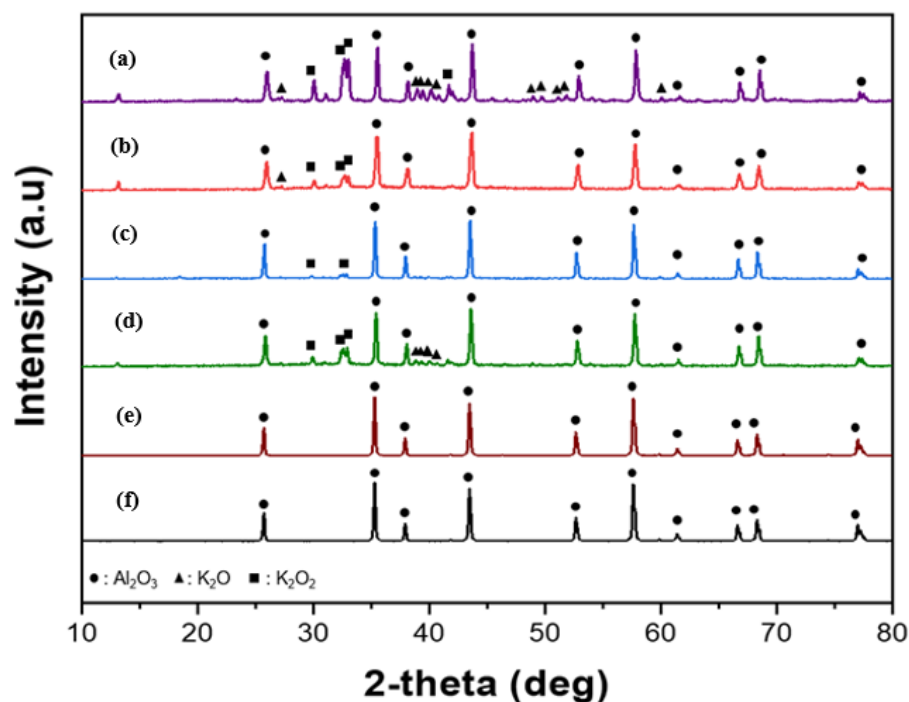


Figure 2. XRD patterns for (a) powder Al_2O_3 , (b) beads Al_2O_3 , (c) powder $\text{KOH}/\text{Al}_2\text{O}_3$, (d) beads $\text{KOH}/\text{Al}_2\text{O}_3$, (e) powder $\text{K}_2\text{CO}_3/\text{Al}_2\text{O}_3$, and (f) beads $\text{K}_2\text{CO}_3/\text{Al}_2\text{O}_3$.

2.2. XRD Analysis of $\text{K}_2\text{O}_2/\text{Al}_2\text{O}_3$ and $\text{K}_2\text{O}/\text{Al}_2\text{O}_3$ Catalysts

The crystallinity and phase transition of powder Al_2O_3 , beads Al_2O_3 , powder $\text{KOH}/\text{Al}_2\text{O}_3$, beads $\text{KOH}/\text{Al}_2\text{O}_3$, powder $\text{K}_2\text{CO}_3/\text{Al}_2\text{O}_3$, and beads $\text{K}_2\text{CO}_3/\text{Al}_2\text{O}_3$ samples were studied by using XRD. As shown in Figure 2, there are ten peaks observed at $2\theta = 26^\circ, 35^\circ, 38^\circ, 44^\circ, 53^\circ, 58^\circ, 62^\circ, 67^\circ, 69^\circ,$ and 78° which corresponded to the Al_2O_3 (JCPDS file 51-0769). The intensity of the support (beads and powder) increase after KOH and K_2CO_3 are deposited onto the surface of the support. In general, all catalysts possessed high crystallinity, indicated by the high intensity and sharp peaks. Based on (Figure 2c,f), all catalysts show same plot for the presence of K_2O_2 at $2\theta = 31^\circ, 33^\circ,$ and 34° (JCPDS file 50-05241) except for $\text{K}_2\text{CO}_3/\text{Al}_2\text{O}_3$ beads (Figure 2f) which show additional K_2O_2 spotted at $2\theta = 43^\circ$ (JCPDS file 50-05241). For K_2O , it was found that the species spotted at $2\theta = 22^\circ, 39^\circ, 40^\circ, 41^\circ,$ and 42° for $\text{KOH}/\text{Al}_2\text{O}_3$ powder (Figure 2c) and another K_2O spotted at $2\theta = 47^\circ, 48^\circ, 49^\circ,$ and 50° for $\text{K}_2\text{CO}_3/\text{Al}_2\text{O}_3$ beads (Figure 2f) (JCPDS file 50-1327). The intensity peaks of beads $\text{KOH}/\text{Al}_2\text{O}_3$ and powder $\text{K}_2\text{CO}_3/\text{Al}_2\text{O}_3$ seem to decrease compared to others due to the hindrance of the higher amount of K disperse on the surface of the catalyst [29]. In this study, powder $\text{KOH}/\text{Al}_2\text{O}_3$ and beads $\text{K}_2\text{CO}_3/\text{Al}_2\text{O}_3$ catalyst was successfully converted to desired species (K_2O_2 and K_2O) for the reaction.

2.3. Catalyst Surface Characteristics

Pore size distribution curves and nitrogen adsorption-desorption isotherm graph for powder Al_2O_3 , beads Al_2O_3 , powder $\text{KOH}/\text{Al}_2\text{O}_3$, beads $\text{KOH}/\text{Al}_2\text{O}_3$, powder $\text{K}_2\text{CO}_3/\text{Al}_2\text{O}_3$, and beads $\text{K}_2\text{CO}_3/\text{Al}_2\text{O}_3$ samples are shown in Figure 3. The BET surface area, total pore volume and average pore diameter are shown in Table 1. It was observed that the BET surface area of all catalysts decreases as compared to Al_2O_3 powder and beads support. Surface area for powder $\text{KOH}/\text{Al}_2\text{O}_3$ and $\text{K}_2\text{CO}_3/\text{Al}_2\text{O}_3$ decrease from $2.45 \text{ m}^2/\text{g}$ to $2.36 \text{ m}^2/\text{g}$ and $1.51 \text{ m}^2/\text{g}$, respectively. For beads catalyst, surface area for $\text{KOH}/\text{Al}_2\text{O}_3$ and $\text{K}_2\text{CO}_3/\text{Al}_2\text{O}_3$ decrease from $282.10 \text{ m}^2/\text{g}$ to $133.37 \text{ m}^2/\text{g}$ and $199.94 \text{ m}^2/\text{g}$, respectively. It was suspected that the surface of catalyst support was covered by potassium compounds, and the pore of the catalyst was blocked [32]. M.A Mohammed et al. [33] also stated that the reduction of the

surface area might be due to the sintering effect that led to particle growth and crystallization. On the other hand, the pore sized of KOH/ Al_2O_3 and K_2CO_3 / Al_2O_3 catalyst increased, as observed in Figure 3.

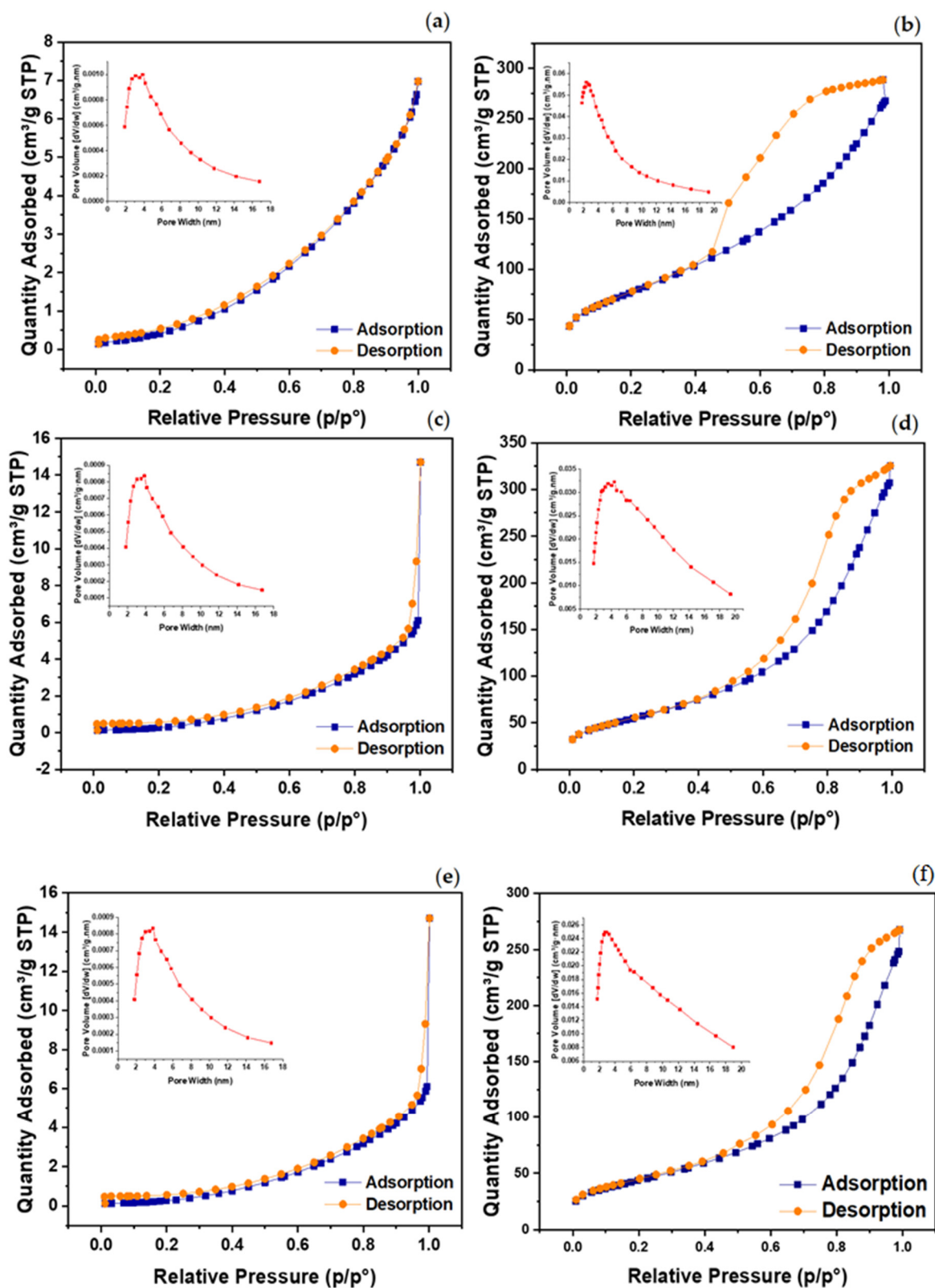


Figure 3. N₂ adsorption-desorption equilibrium and BJH pore size distribution of (a) powder Al_2O_3 , (b) beads Al_2O_3 , (c) powder KOH/ Al_2O_3 , (d) beads KOH/ Al_2O_3 , (e) powder K_2CO_3 / Al_2O_3 , and (f) beads K_2CO_3 / Al_2O_3 catalyst.

Table 1. Physical properties of alumina-based K₂CO₃ and KOH catalyst with its mass content and density of active sites.

Catalyst	Physical Properties			Mass of Element (%)			Density of Active Site (mmol/g)		
	Surface Area (m ² /g) ¹	Pore Volume (cm ³ /g) ²	Pore Size (nm) ²	K	O	Al	Weak (<160 °C)	Moderate (160–400 °C)	Strong (>400 °C)
powder Al ₂ O ₃	2.50	0.01	5.03	0.00	0.00	99.98	2.36	-	-
beads Al ₂ O ₃	282.10	0.44	6.24	0.00	0.00	99.98	0.34	0.20	0.45
powder KOH/Al ₂ O ₃	2.40	0.01	5.16	22.50	45.26	32.24	N/A	N/A	N/A
beads KOH/Al ₂ O ₃	133.40	0.35	7.09	25.37	41.48	33.15	0.15	0.08	2.38
powder K ₂ CO ₃ /Al ₂ O ₃	1.506	0.0069	5.437	18.96	43.27	37.77	N/A	N/A	N/A
beads K ₂ CO ₃ /Al ₂ O ₃	199.94	0.474	6.512	28.41	45.44	26.15	0.00	0.17	3.94

¹ BET surface area; ² estimated from Barrett, Joyner, and Halenda (BJH) model.

All four catalysts and supports that have narrow pore size distribution with diameter in between ~5 and ~7 nm are displayed in Figure 4c–f and summarized in Table 1. Pore sizes for Al₂O₃ powder and beads support were 5.03 and 6.24 nm, respectively and the broad peak of pore distribution is displayed in Figure 3a,b. When KOH and K₂CO₃ are immobilized onto the surface of the Al₂O₃ powder support, the pore size increases to 5.15 nm and 5.44 nm, with both catalysts seem to have similar pore distribution with Al₂O₃ powder support (Figure 3c,e). For Al₂O₃ beads support, the better pore distribution was spotted after KOH and K₂CO₃ were immobilized onto the surface of the Al₂O₃ beads support (Figure 3d,f). Beads KOH/Al₂O₃ and K₂CO₃/Al₂O₃ seem to have wider pore distribution and better pore size making the catalyst much effective and efficient. As shown in Figure 3 all catalyst displayed type V (based on IUPAC classification) isotherms for the typical H₃ hysteresis loop for powder catalyst and H₄ hysteresis loop for beads catalyst, validating the existence of mesoporous characteristics (2–50 nm based on IUPAC) [34] in the channel. Based on the isotherm plot in Figure 3, if the adsorption-desorption reaction occurs in relative pressure (p/p^o) of 0.4 to 0.6 is generally attributed to small pores [35]. The KOH/Al₂O₃ powder, KOH/Al₂O₃ beads, K₂CO₃/Al₂O₃ powder, and K₂CO₃/Al₂O₃ beads samples show a hysteresis effect in the 0.4 to 0.6 relative pressure region, which is characteristic of small pore texture. Powder catalyst has small pore texture and small surface area while beads catalyst shows smaller pore texture and large surface area based on the hysteresis loop [36]. Beads catalysts seem to be the best catalyst as the surface area, pore size, and pore distribution are better than powder catalysts.

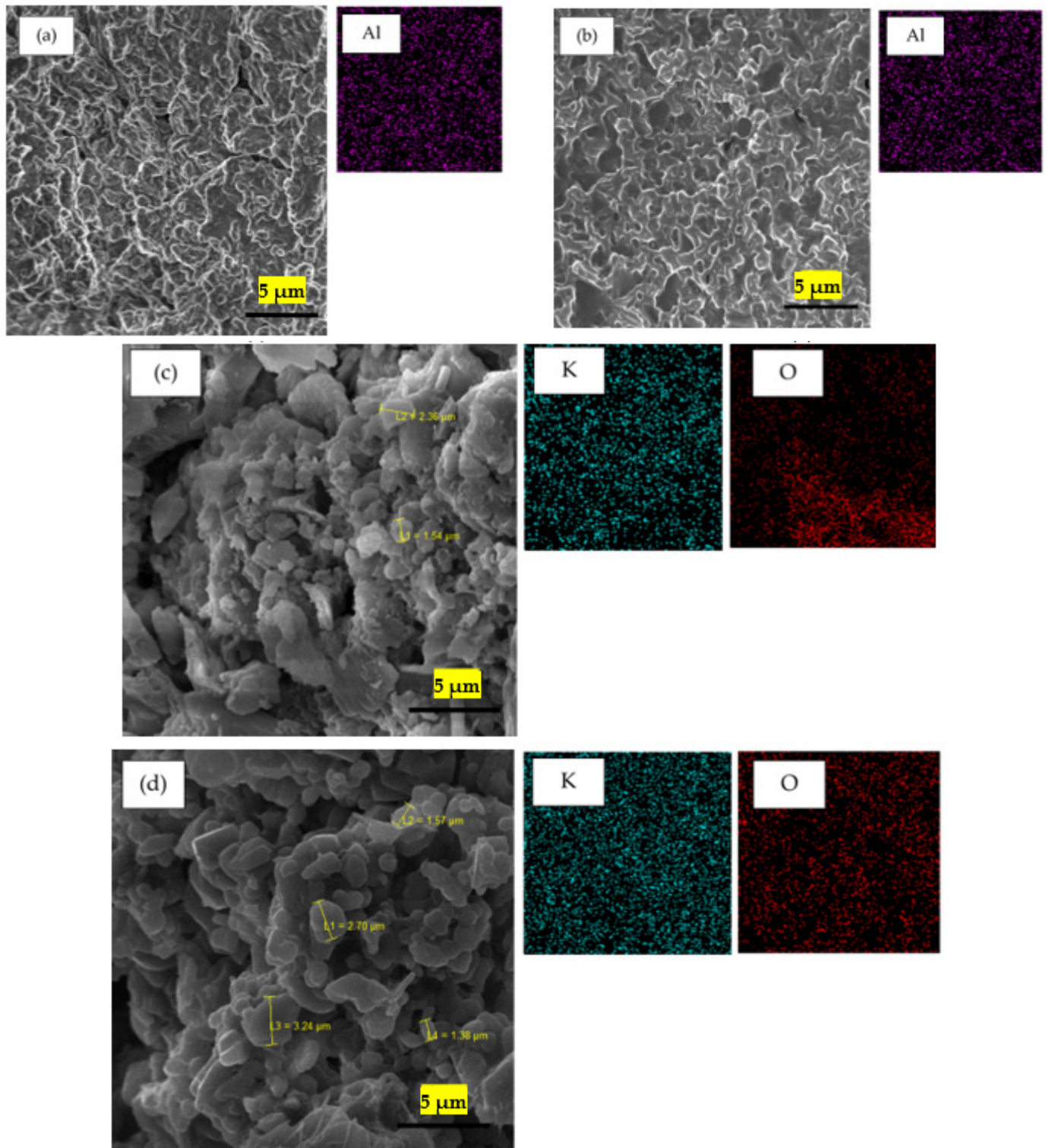


Figure 4. Cont.

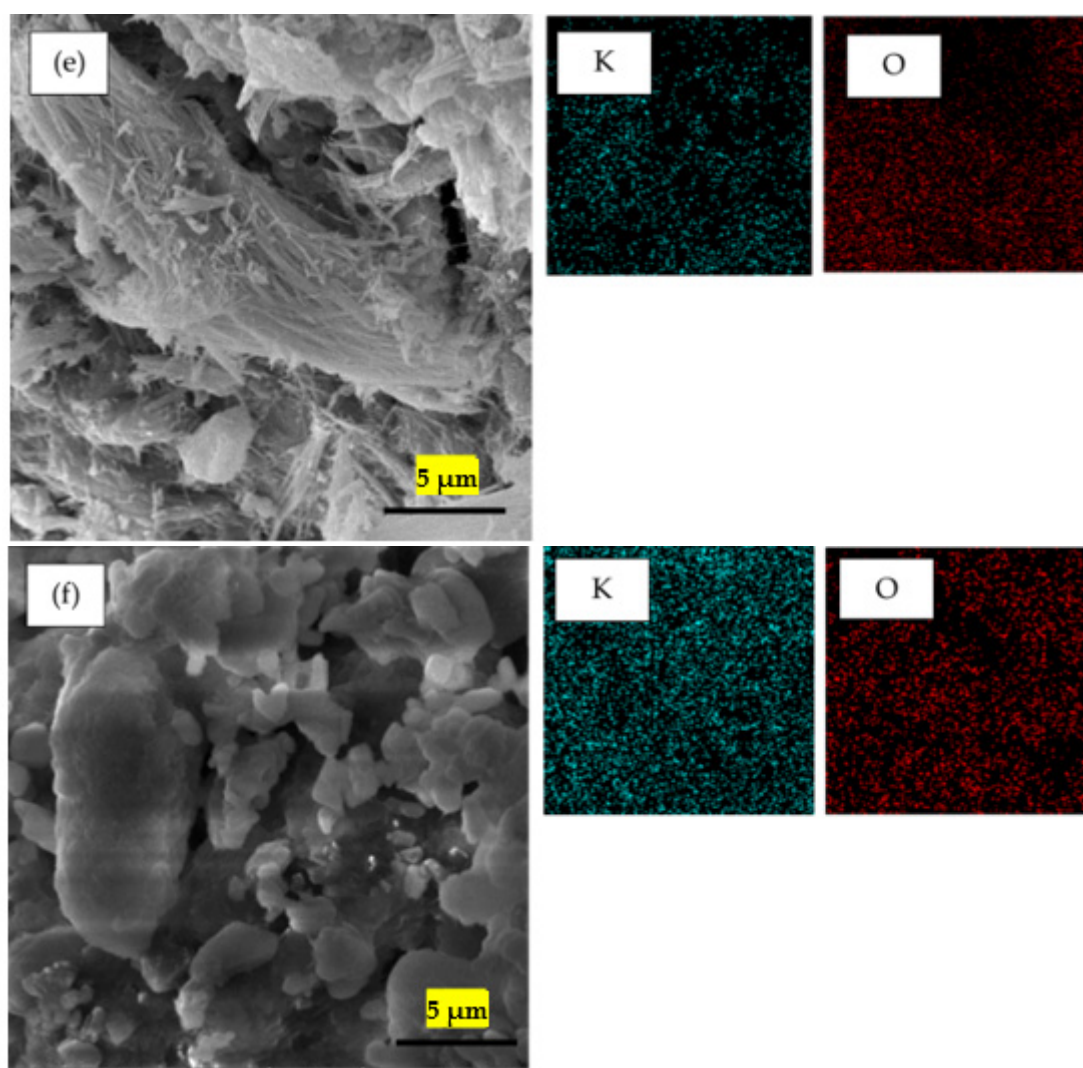


Figure 4. SEM images and EDX mapping for (a) powder Al_2O_3 , (b) beads Al_2O_3 , (c) powder $\text{KOH}/\text{Al}_2\text{O}_3$, (d) beads $\text{KOH}/\text{Al}_2\text{O}_3$, (e) powder $\text{K}_2\text{CO}_3/\text{Al}_2\text{O}_3$, and (f) beads $\text{K}_2\text{CO}_3/\text{Al}_2\text{O}_3$.

2.4. Scanning Electron Microscope—Energy Dispersive X-ray Analysis

Figure 4 shows the SEM images of Al_2O_3 , $\text{KOH}/\text{Al}_2\text{O}_3$, and $\text{K}_2\text{CO}_3/\text{Al}_2\text{O}_3$ catalyst with the EDX mapping of potassium (K) and oxygen (O). It was observed that the morphology of alumina-based K_2CO_3 and KOH catalysts exhibited a relatively tight irregular plate structure. For powder $\text{K}_2\text{CO}_3/\text{Al}_2\text{O}_3$ (Figure 4e), the appearance of a large oval shape-like fibrous plate on the surface is due to the agglomeration of the catalyst in addition to the exfoliation of its surface. Compared to the beads catalyst (Figure 4d,f), the irregular plate image can be clearly observed and showed a good morphological structure with higher surface area as recorded by BET data in Table 2.

Table 2. The reusability study for beads catalyst with and without PHM.

Catalyst	Reusability							
	1st	2nd	3rd	4th	5th	6th	7th	8th
$\text{K}_2\text{CO}_3/\text{Al}_2\text{O}_3$ (PHM)	77.4	70.2	66.7	55.7	43.6	40.2	19.5	0
$\text{K}_2\text{CO}_3/\text{Al}_2\text{O}_3$	72.1	0	0	0	0	0	0	0
$\text{KOH}/\text{Al}_2\text{O}_3$ (PHM)	86.8	70.6	0	0	0	0	0	0
$\text{KOH}/\text{Al}_2\text{O}_3$	73.5	0	0	0	0	0	0	0

Saba et al. [28] stated that the strong basic properties of the catalyst of K_2CO_3/Al_2O_3 have a high potential to absorb moisture resulting from particle agglomeration.

This observation is consistent with the data in Table 1, where the structure is mesoporous with a high surface area. Based on the mapping images of the EDX, the distribution of elements K and O revealed significant dispersion on the surface of the Al_2O_3 support material. It was observed that the distribution of K and O on the beads Al_2O_3 has better uniformity as compared to powder catalyst. This finding is in good agreement with the research reported by A. Islam et al. [34] where they reported that the potassium element has good dispersion on the surface of the beads Al_2O_3 catalyst.

2.5. Temperature Programmed Desorption-Carbon Dioxide Analysis

The strength and proportion of the different basic sites of the catalyst need to be evaluated by thermal desorption of CO_2 (CO_2 -TPD). Figure 5 shows the TPD- CO_2 profile of calcined material for beads Al_2O_3 , KOH/Al_2O_3 , and K_2CO_3/Al_2O_3 with the amount of CO_2 desorbed (mV) as a function of the CO_2 desorption temperature ($^{\circ}C$). The higher CO_2 desorption peak indicates the highest catalyst basicity because the strength of the surface bond reflects the temperature at which the CO_2 is desorbed, resulting in peaks that can be correlated to three different types of active sites. The three different types of strength active sites reported by Junior et. al. and Shan et. al. [18,37] were weak sites (CO_2 desorbed $<160^{\circ}C$), medium sites (CO_2 desorbed $160^{\circ}C < x < 400^{\circ}C$), and strong site (CO_2 desorbed $>400^{\circ}C$). Then, according to the attained desorption temperature, beads Al_2O_3 show medium desorption peak range $90^{\circ}C$ to $384^{\circ}C$ (highest peak at $270^{\circ}C$). The peak was assigned by the presence of SiO_2 , where it was used as the binder to keep the sphere structure of supports and enhanced basic properties of catalyst [38]. For beads, KOH/Al_2O_3 catalyst shows a strong and broad desorption peak range $350^{\circ}C$ to $800^{\circ}C$ (peak at $536^{\circ}C$). This broadband indicated the presence of covalent bonding between CO_2 and K/Al_2O_3 [32]. However, the K_2CO_3/Al_2O_3 has broad peaks from $350^{\circ}C$ to $850^{\circ}C$, peaked at $764^{\circ}C$ with two small shoulders at $524^{\circ}C$ and $630^{\circ}C$. Within that range, between 350 and 580 indicates low strength, in between 580 and 697 indicates medium strength, and 700 and 860 indicates high strength [39–41]. Furthermore, it was observed that K_2CO_3/Al_2O_3 has 3.94 mmol/g of basic sites, and KOH/Al_2O_3 has 2.38 mmol/g of basic sites. From this data, K_2CO_3/Al_2O_3 has higher basic sites and is predicted to be a high performance of catalyst for biodiesel production. TPD- CO_2 findings were in agreement with BET data in Table 2 in regards to the increased basicity due to the higher surface area (higher active sites) [41]. Despite the similarity between the physical properties of beads and powder catalysts, beads catalyst remains a better choice.

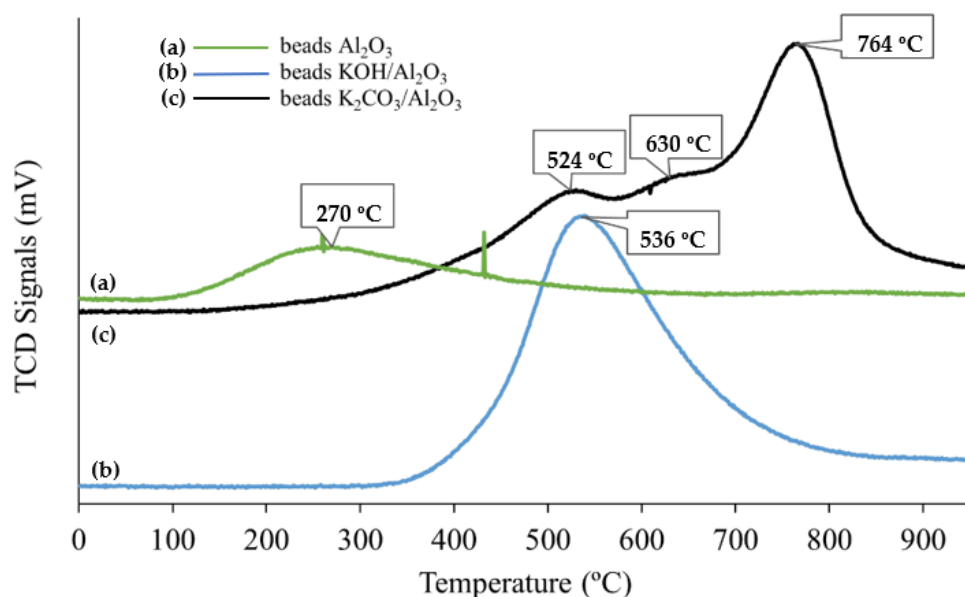


Figure 5. TPD- CO_2 profile of calcined material for beads Al_2O_3 , beads $\text{KOH}/\text{Al}_2\text{O}_3$, and beads $\text{K}_2\text{CO}_3/\text{Al}_2\text{O}_3$.

2.6. Transesterification Reaction

Further analysis on the sample was conducted by using GC-MS to calculate the actual pure FAME content from the impure biodiesel collected from transesterification reaction where the percentage of ester content was obtained. Methyl heptadecanoate (C17) was used as the internal standard in the analysis to calculate the ester content based on the peak area of FAME species in the sample relative to the standard [42]. The ester content was calculated using formula (2) as mentioned in Section 2.6 (EN14103). Sample from beads $\text{K}_2\text{CO}_3/\text{Al}_2\text{O}_3$ catalyst at 1 h reaction time was tested for GCMS qualitative analysis, and from the result in Figure 6, eight peaks were observed for the entire compound present in the biodiesel, of which only seven corresponded to the methyl ester group [43]. The identified FAME was analyzed against the standard peak from pure biodiesel sample (internal standard) of myristate methyl ester, palmitate methyl ester, stearate methyl ester, oleate methyl ester, linoleate methyl ester, linolenate methyl ester, and heptadecanoic acid methyl ester. All peaks that appeared (except for 9-hexadecanoic acid) were verified against different esters and confirmed using the mass spectroscopy (MS) library programmed. Furthermore, a standard sample (100% pure biodiesel) was tested and used as a benchmark for the selection of the right peaks to calculate the ester contained in the collected biodiesel [42].

The results of biodiesel yield are shown in Figure 7. The experiments were carried out using a catalyst containing 30% $\text{KOH}/70\% \text{Al}_2\text{O}_3$ and 30% $\text{K}_2\text{CO}_3/70\% \text{Al}_2\text{O}_3$. The optimum condition for the transesterification reaction was 1:12 of oil to methanol ratio, 5 wt% of catalyst loading, 65 °C of reaction temperature, and 1 to 4 h reaction time. According to the results, powder $\text{KOH}/\text{Al}_2\text{O}_3$ catalyst shows 66.7% biodiesel yield at 3 h reaction time, and powder $\text{K}_2\text{CO}_3/\text{Al}_2\text{O}_3$ catalyst shows 72.28% biodiesel yield at 4 h reaction time. In comparison, beads catalyst exhibited the highest biodiesel yield which beads $\text{KOH}/\text{Al}_2\text{O}_3$ catalyst shows 86.8% biodiesel yield at 2 h reaction time and powder $\text{K}_2\text{CO}_3/\text{Al}_2\text{O}_3$ catalyst shows 77.3% biodiesel yield at 2 h reaction time. This result is coherent with BET and TPD results where beads catalyst provides larger surface area (refer to Table 1) that increases many active sites deposited on the surface and increasing the basicity of the catalyst. The lack of performance of powder catalyst can be divided into two, which are either the catalyst is easily coated by glycerol as the catalyst and glycerol at the bottom of the container or direct contact between the catalyst and magnetic stirrer resulting in deactivation of the catalyst [44,45]. Moreover, a study from [34] stated that increasing the reaction time will ultimately increase the effect of the leaching of the powder

catalyst. The catalyst that can produce biodiesel more than 70% can be considered a good catalyst, as industrial production in Malaysia using homogeneous catalysts can produce biodiesel up to 65% to 85% per batch. Beads catalysts for both K_2CO_3 and KOH remain a better choice for increased biodiesel production compared to the powder catalyst. In comparison, research studied by Shan et. al. [37], produce biodiesel from palm oil catalyzed by palygorskite-supported K_2CO_3 resulting in 75–85% biodiesel yield at 2 h reaction time.

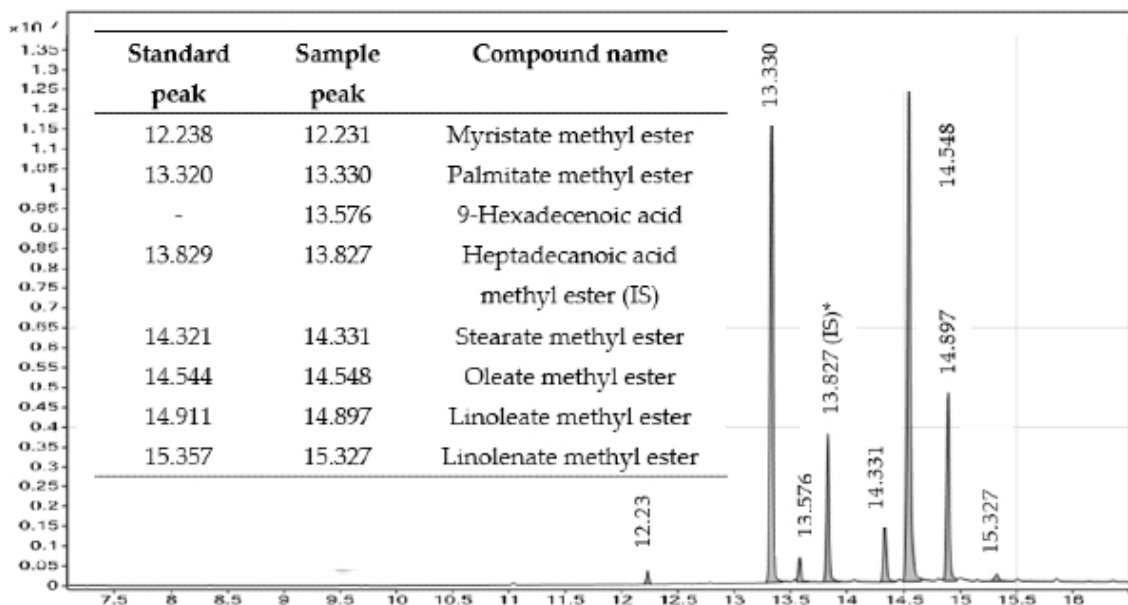


Figure 6. Example of GC-MS intensity peak area and compound of each peak for K_2CO_3/Al_2O_3 beads catalyst. * (IS) Internal Standard.

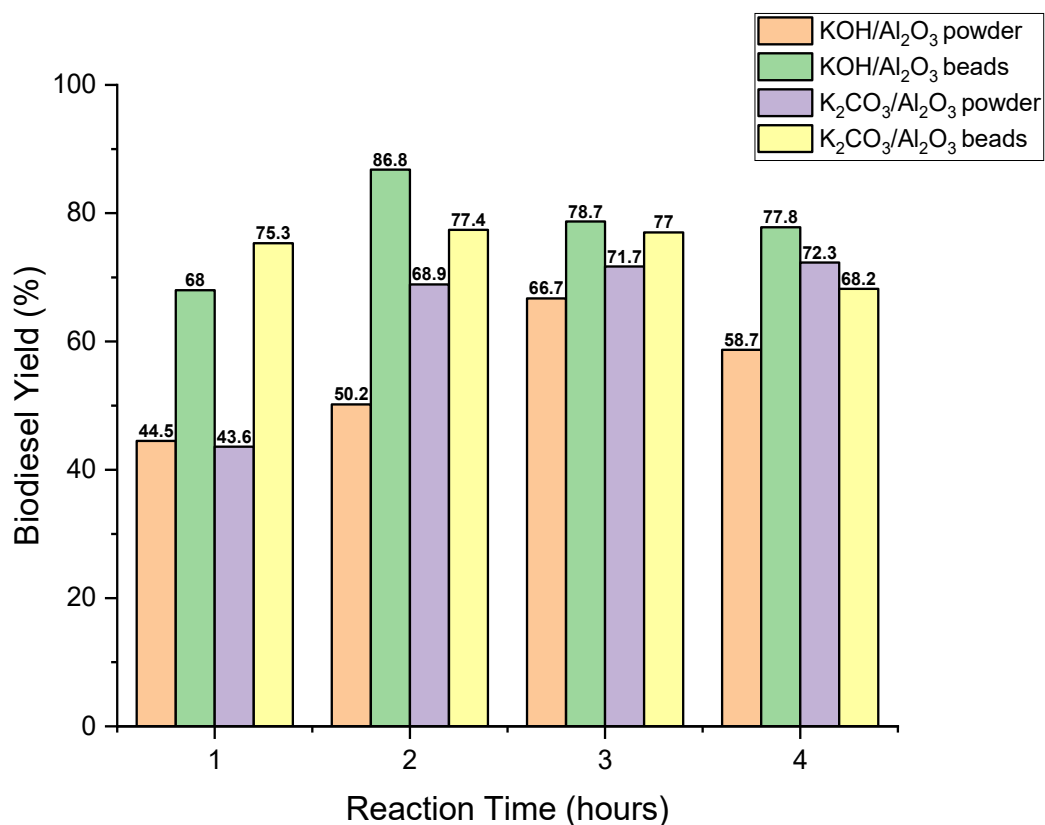


Figure 7. Percentage yield of pure biodiesel.

2.7. Reusability Testing for Beads $\text{KOH}/\text{Al}_2\text{O}_3$ and $\text{K}_2\text{CO}_3/\text{Al}_2\text{O}_3$

$\text{K}_2\text{CO}_3/\text{Al}_2\text{O}_3$ and $\text{KOH}/\text{Al}_2\text{O}_3$ (beads and powder) catalysts that reveal the highest yield in Section 2.6 then underwent reusability testing to obtain the stability information of the catalyst after a few cycles of reaction. Beads formed of both catalysts were proceed at 2 h reaction time while for powder $\text{K}_2\text{CO}_3/\text{Al}_2\text{O}_3$ catalyst at 4 h reaction time and $\text{KOH}/\text{Al}_2\text{O}_3$ catalyst at 3 h reaction time. The catalyst recovered after the reaction was washed and reactivated at 700 °C for 2 h. By washing and reactivating the catalyst, the impurities that remained on the catalyst's surface were removed, and the active sites were exposed for another reaction. The reusability testing was performed up to the 7th cycle for $\text{K}_2\text{CO}_3/\text{Al}_2\text{O}_3$ beads catalyst and 2nd cycle for $\text{KOH}/\text{Al}_2\text{O}_3$ beads catalyst by maintaining the amount of catalyst for every cycle in order to cover up the loss of the catalyst amount during the separation and reactivation process. From the experiment, the mass for the spent catalyst remains unchanged and Figure 8 reveals that there was a slight decrease in the pattern in the biodiesel yield. However, the conversions were still considered as high until the second cycle. For $\text{KOH}/\text{Al}_2\text{O}_3$ beads and powder catalyst, the reusability of the catalyst stops at the third cycle because the catalyst becomes soggy and ruptures due to the hygroscopic characteristic of the material [14,46]. The $\text{K}_2\text{CO}_3/\text{Al}_2\text{O}_3$ catalyst shows tremendous performance in converting the biodiesel. The strong and stable structure makes the catalyst very useful until the last cycle. In the end, the reason for declining biodiesel conversion might be due to the leaching of K_2O_2 and K_2O from Al_2O_3 , resulting in the loss of active sites from the surface of the catalyst [47,48].

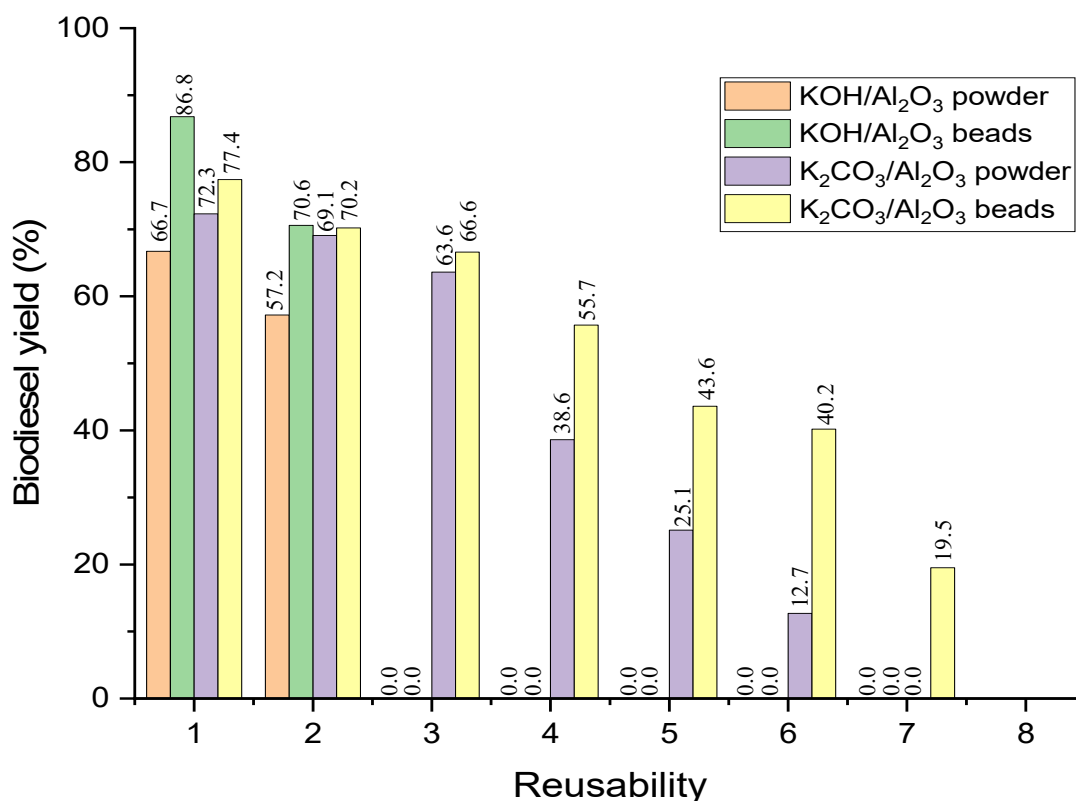


Figure 8. Reusability testing for $\text{K}_2\text{CO}_3/\text{Al}_2\text{O}_3$ and $\text{KOH}/\text{Al}_2\text{O}_3$ catalyst.

The reusability study for comparison between beads catalyst with and without using PHM is tabulated in Table 2. PHM shows an excellent contribution by preventing the occurrence of cracks coupled with maintaining the shape of the catalyst until 7th catalyst cycle. The disadvantages without using PHM that has been studied in this project are (i) the beads catalyst have high potential to crack due to the direct contact with the magnetic stirrer and (ii) the catalyst leaches out from the support after a few catalytic cycles. A

previous study conducted by [31] used K_3PO_4 supported-alumina beads and revealed that the reusability of the catalyst was up to the 2nd cycle, as leaching effect resulting from the crushed beads catalyst becomes apparent at the 3rd cycle.

2.8. Identification of Post-Reaction Compounds on the Catalyst Surface Using Fourier-Transform Infrared Spectroscopy

The beads K_2CO_3/Al_2O_3 and beads KOH/Al_2O_3 catalysts were chosen and favored over others due to their high biodiesel production and reusability. Thus, further investigation was carried out to identify the compounds present in the spent catalyst using FTIR and compared with fresh beads K_2CO_3/Al_2O_3 and KOH/Al_2O_3 catalysts. The catalysts showed sample adsorption of wavelength, with the observation of higher adsorption intensity of beads KOH/Al_2O_3 catalyst compared to beads K_2CO_3/Al_2O_3 catalyst. This implies that the catalyst can easily degenerate after yielding low biodiesel for few consecutive cycles and then become unrecyclable. This may be attributed to the presence of an undesired compound on the surface of the catalyst after the reaction. The compound probably binds permanently to the surface of the catalyst and inhibit the performance of active sites. The catalyst may also be leached out from the support, thereby reducing the catalyst performance.

Figure 9 shows the FTIR spectrum of the fresh and spent catalyst after 2nd cycle for KOH/Al_2O_3 and 7th consecutive cycle for K_2CO_3/Al_2O_3 , resulting in the degeneration of the potential catalyst. From the FTIR spectrum, the fresh catalyst for KOH/Al_2O_3 and K_2CO_3/Al_2O_3 shows straight lines indicating that there is no species/impurities found on the surface of the catalyst compared to the spent catalyst. For the spent catalyst, it was presented that the strong hydroxyl (ν -OH) stretching vibration of the surface of the hydroxyl group that attached to the catalyst can be observed at the wavelength range of 3500 to 3200 cm^{-1} [44]. For sp^3 and sp^3 aliphatic hydrocarbon chain (ν -CH) for stretching vibration can be observed at a wavelength of 3000 to 2820 cm^{-1} and 2750 cm^{-1} , respectively [49,50]. The carbonyl group (ν -C=O) stretching vibration of 1735 cm^{-1} and continue adsorption at wavelength of 1600 cm^{-1} due to aliphatic alkene structure (ν -C=C) were caused by fatty acids methyl ester [51,52]. The hydroxyl (ν -OH) bending vibration occurs at 1550 caused by H_2O adsorbed from the air [44]. The vibration of a cyclic compound such as benzene rings (ν -C=C) and the major absorption peak at the wavenumber of 1407 cm^{-1} can be assigned to the asymmetric stretching of carbonate (ν - CO_3^{2-}) group observed in the K_2CO_3 calcined at 700 °C. The resonance of the carbon bond atom with an oxygen atom (ν -CO, ν -C=C, and ν -COC) can be observed at a range of 1600 to 1200 cm^{-1} and continue at a range of 1100 to 1000 cm^{-1} , respectively [53–55]. The lower frequency basically shows the properties of the metal oxide where the range 1000 to 700 cm^{-1} indicates the strong bending of a carbonyl compound with metal ions (ν -CO- X^+) where X represents the potassium ion (K) [37,56]. As shown in Figure 9, the spent catalyst shows the formation of a new peak that might be coming from the impurities or side product at the end of the reaction. Surprisingly, as can be seen from the catalyst's figure, the potential beads catalyst retains its shape and can overcome the mass loss problem from the catalyst caused by cracking or flushing away of the catalyst together with the reagent used in the reaction. This statement is supported by the TGA result in Figure 1, where the catalyst shows good stability even calcined at higher temperatures. The next observation found was the catalyst changes its color from white to dark orange gradually in every cycle. The spent catalyst changes its color because of the poisoning effect by the side product of the reaction [27,57,58], which is glycerol. During the separation process, glycerol has a dark red color and the side product was located at the bottom of the flask mixed with beads catalyst [59] through the PHM. At the end of 7th catalytic cycle, the physical appearance of the catalyst shows a crack layer for some beads due to the vibration and collision with a magnetic stirrer which reduces the catalyst's performance [60]. Moreover, the K_2O and K_2O_2 have difficulties from water molecules (H_2O) during the reaction because the catalyst reacts with sorbed water from the sample by physical adsorption [34] and causes the bending of OH radical ($>1650\text{ cm}^{-1}$) and formation of glycerol carbonate (1800–1000 cm^{-1}) [14].

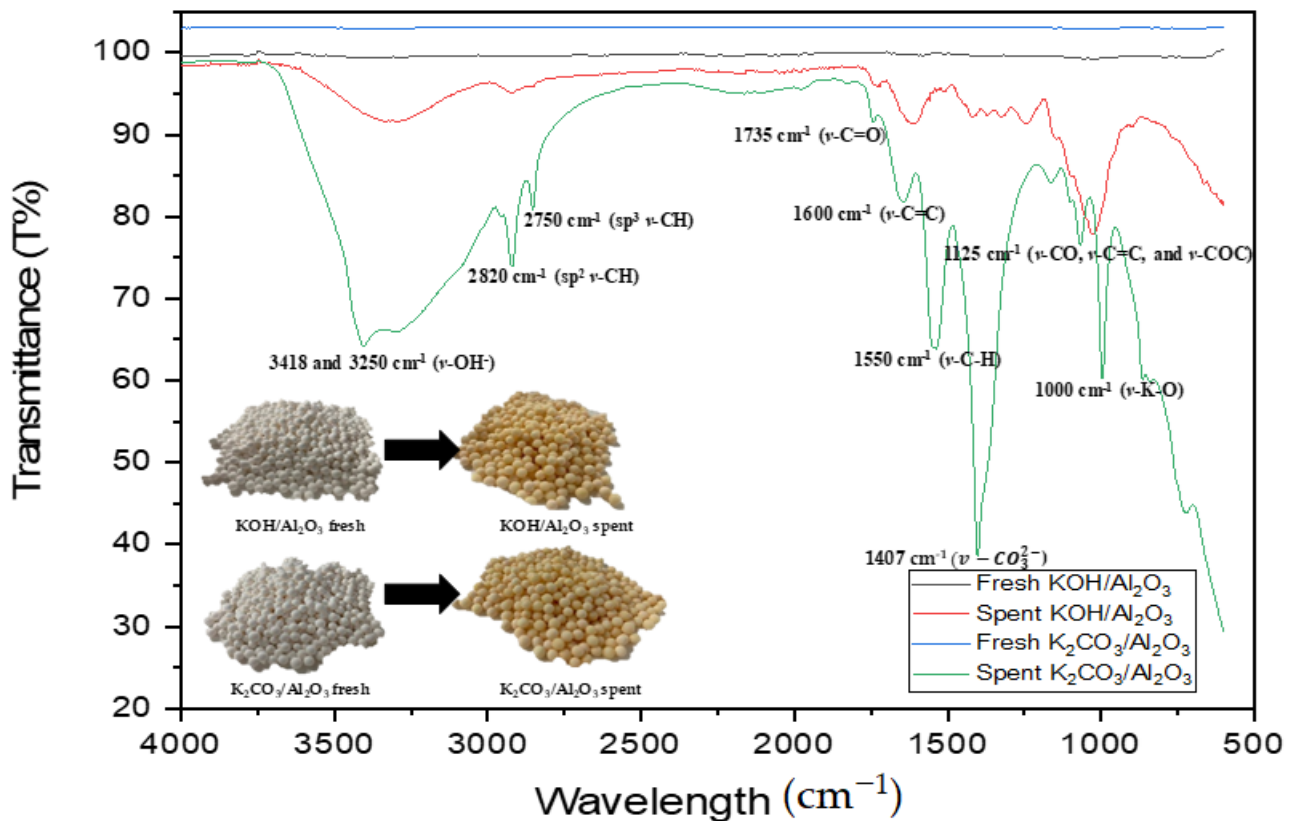


Figure 9. FTIR spectrum of fresh KOH/Al₂O₃ catalyst; fresh K₂CO₃/Al₂O₃ catalyst; spent beads K₂CO₃/Al₂O₃ catalyst; and spent beads KOH/Al₂O₃ catalyst.

2.9. XRF and ICP-AES Analysis

Spent beads K₂CO₃/Al₂O₃ catalyst were chemically analyzed by means of X-ray fluorescent spectrometry (XRF) as mentioned in Table 3. The inductively coupled plasma atomic emission spectroscopy (ICP-AES) was carried out to study the element present in the biodiesel liquid, and the data are shown in Table 4. The XRF and ICP-AES data were obtained only for 1st, 4th, and 8th cycles. According to the results of analyses, it was detected that the leaching happens on the surface of the catalyst—the number of elements that leach out from the surface does not exceed 7%. The previous study also reported that using potassium-based catalyst resulted in the lowest percent of leaching [61] and is easy to recover as the catalyst has defined shape and is larger in size. These data have an agreement with ICP-AES where the catalyst performance starts to drop at the 8th cycle.

Table 3. XRF analysis results of used beads K₂CO₃/Al₂O₃ catalyst in the transesterification process.

Element Analyzed	Fresh (%)	1st Cycle (%)	4th Cycle (%)	8th Cycle (%)
Potassium, (K)	0.21	0.97	4.3	6.3
Aluminum, (Al)	0.00	0.02	0.05	2.4
Others	0.03	1.03	1.52	2.0

Table 4. Chemical analysis by ICP-AES of biodiesel liquid sample by using beads K_2CO_3/Al_2O_3 catalyst in the transesterification process.

Element Analyzed	1st Cycle (%)	4th Cycle (%)	8th Cycle (%)
Potassium, (K)	1.0	3.3	6.4
Aluminum, (Al)	0.0	0.1	1.5

3. Materials and Methods

3.1. Materials

The WCO was obtained from Pasir Gudang, Johor, Malaysia. The pre-treated process started when the WCO bottle was heated first on a hot water bath to dissolve all saturated fat that was deposited at the bottom of the bottle. After that, WCO was filtered to remove traces such as suspended solids and WCO was transferred to the beaker and it was heated at 100 °C on a hotplate for 1 h to remove traces of water, followed by preliminary analysis; acid value (AV) (ASTM D664/D8045-17e1), saponification value (SV) (ASTM D94), free fatty acids content (FFA) (ASTM D5555-95), viscosity (ASTM D445/D446), and moisture content (ASTM D5556-19). Meanwhile, the beads alumina oxide (Al_2O_3) (particle size < 5 mm), and powder Al_2O_3 (particle size < 1mm), the analytical grade (AR) methanol (CH_3OH , purity 99%), phenolphthalein ($C_{20}H_{14}O_4$, purity 99%), and methyl heptadecanoate ($C_{18}H_{36}O_2$, purity 99%) as the internal standard for biodiesel were purchased from Sigma-Aldrich (Selangor, Malaysia). The potassium carbonate (K_2CO_3 , purity 99%), potassium hydroxide (KOH, purity 99%), sodium hydroxide (NaOH, purity 99%), and hydrochloric acid (HCl) (32% concentration, purity 97%) were obtained from Merck (Selangor, Malaysia) chemical company. Meanwhile, the container for the catalyst in the reaction medium (Figure 10) was made from low-density polyethylene (LDPE) of perforated hydrophilic materials (PHM).

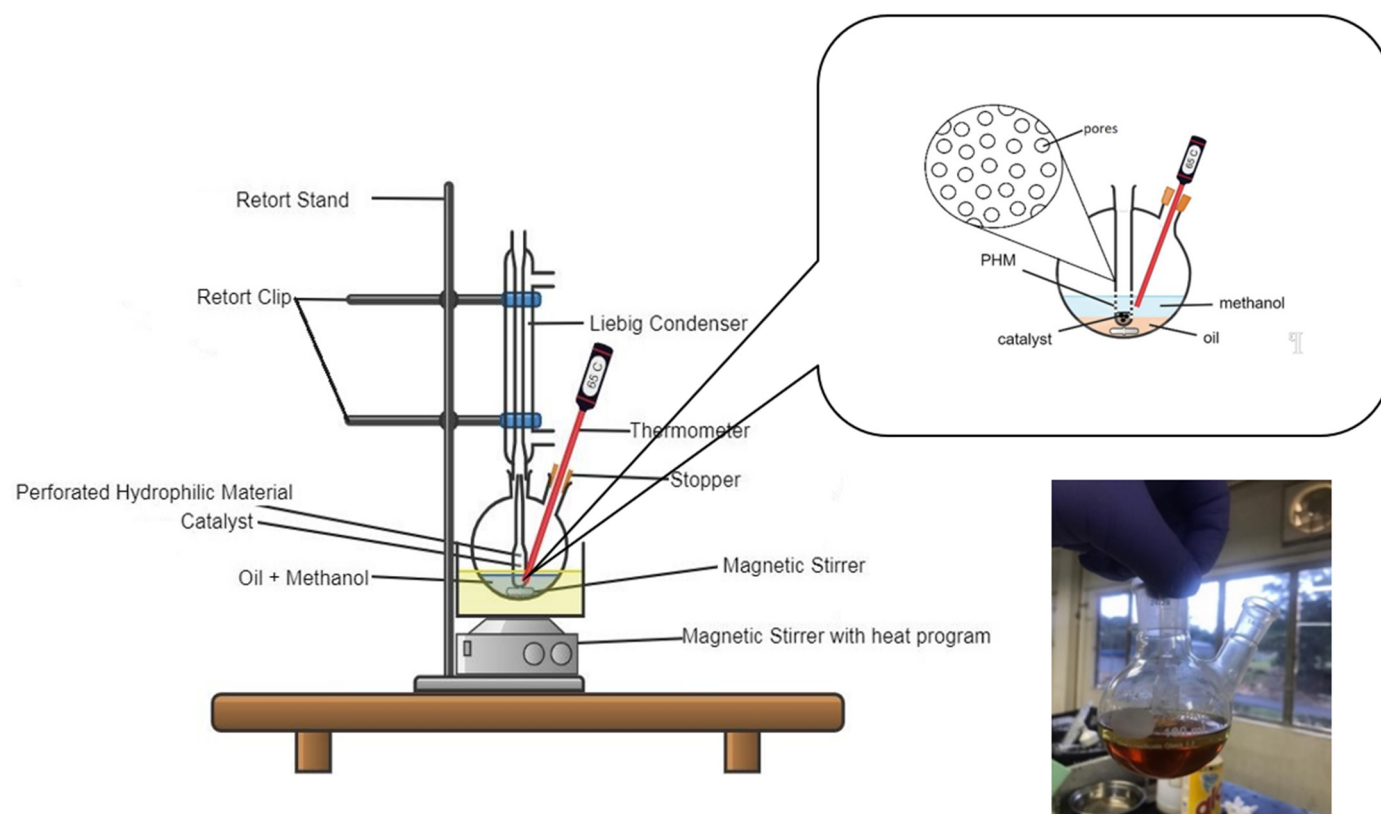


Figure 10. Schematic design of the open-system reactor for the transesterification process with the application of the fabricated PHM porous catalyst container.

3.2. Preparation of K_2CO_3 and KOH/Al_2O_3 Catalysts

In this work, both beads and powder catalysts were prepared by incipient wetness impregnation technique. Briefly, K_2CO_3 and KOH salt solutions were added dropwise to water suspension containing powder- Al_2O_3 in the separate beaker. The mixture was stirred and heated at $100\text{ }^\circ\text{C}$ for 5 h, followed by the ageing process at $90\text{ }^\circ\text{C}$ for 24 h, and calcined at $700\text{ }^\circ\text{C}$ for 3 h with ramping $15\text{ }^\circ\text{C min}^{-1}$ to produce powdered K_2CO_3/Al_2O_3 and KOH/Al_2O_3 catalysts. The same procedure was applied to prepare K_2CO_3/Al_2O_3 and KOH/Al_2O_3 catalysts using beads Al_2O_3 as support.

3.3. Catalyst Characterization of K_2CO_3/Al_2O_3 and KOH/Al_2O_3 Catalysts

The TGA-Pyris 2012 thermogravimetric analysis assisted by thermal gas detector GSA7 from Perkin Elmer (Selangor, Malaysia) was used to determine the thermal decomposition of the prepared catalyst. The analysis was carried out in a static air atmosphere at a heating rate of $15\text{ }^\circ\text{C min}^{-1}$. The weight lost and the derivative thermogravimetry (DTG) of the sample against the temperature was plotted.

While the LabX XRD-6100 PANalytical, X-ray diffraction (XRD) analyzer was used for the identification and characterization of the internal structure, bulk phase, and the composition crystallinity phases of the catalyst, the analysis was carried out utilizing X'Pert PRO Theta from PANalytical diffracted beam monochromator, using step scan mode with range $0^\circ - 90^\circ$ of theta (θ) with the scan rate of 2° min^{-1} .

For the quantity, distribution, and strength of the catalyst's active sites, the prepared catalysts were examined using Thermo Finnigan (Selangor, Malaysia), TPDRO 1100 series of carbon dioxide-temperature programmed desorption CO_2 -TPD. The sample was first treated with N_2 and heated up to $150\text{ }^\circ\text{C}$ for 1 h to remove all the particulates and moisture, followed by the absorption of CO_2 gas at 10 cc min^{-1} for 1 h at ambient temperature. The second treatment of the sample was done to remove excess CO_2 gas by flowing the N_2 gas through the samples for another 1 h. Finally, the sample is ready for analysis, and was heated from $50\text{ }^\circ\text{C}$ to $1000\text{ }^\circ\text{C}$ with a heating rate at $10\text{ }^\circ\text{C min}^{-1}$, and the He gas was flowed through the system to carry the CO_2 gas detached from the sample before being detected by the thermal conductivity detector. Finally, the intensity of detected gas molecules was plotted versus the temperature.

N_2 adsorption/desorption isotherm analysis was performed using Micro metrics ASAP 2010 (Selangor, Malaysia) to determine the catalyst surface area, average pore sizes, pore type, and total pore volumes. Prior to the analysis, the sample was degassed and heated for 24 h at $120\text{ }^\circ\text{C}$ to remove moisture and other particulate matter. The N_2 gas was allowed to enter the sample reactor to fill the tube with N_2 molecules. The reactor containing catalyst was a dip into the liquid N_2 to ensure the physisorption attachment of the molecules on the surface of the catalyst. The data isotherms were recorded against the pressure detected to determine the pore volume and surface area of the K_2CO_3 and KOH/Al_2O_3 catalysts.

For the morphological and elemental composition analyses, the TESCAN VEGA3 scanning electron microscopy (SEM), Novatiq scientific Singapore (Selangor, Malaysia) equipped with energy-dispersive X-ray spectroscopy (EDX) was utilized. Before analysis, the sample powder was placed on the sample holder and coated with Au using a TESCAN coater.

To study the stability and the strength of catalyst structure, the spent catalyst was analyzed by Fourier transform infrared spectroscopy (FTIR) model Nicolet Is5 from Thermo Fisher (Selangor, Malaysia). It was used to record the remaining active species present on the catalyst after few cycles of the reaction. The spent catalyst was analyzed by Supermini bench-top sequential wavelength dispersive X-ray fluorescence (XRF) spectrometer in helium (He) atmosphere. Normalized contents of a dominant element were used as a reference and compared to samples recovered after transesterification reaction. The contents were calculated from XRD intensities and analytical apparatus factory calibration data for certain elements. All samples before XRF analysis were ground, sieved to particle size ($x < 0.011\text{ mm}$), and dried at 250° for 6 h. The contents of the main components

on the biodiesel liquid were determined by inductively coupled plasma atomic emission spectroscopy (ICP-AES). The ICP-AES measurements were performed on a Prodigy 7 (Selangor, Malaysia) spectrometer and carried out under optimized experimental con.

3.4. Transesterification Reaction of WCO

The transesterification process was adapted with slight modification from previous research reported by Abdullah et al. [25]. About 10 g of the WCO was added to a 50 mL two-necked round bottom flask, heated to 65 °C and subsequently added with 4.32 g methanol with oil to methanol molar ratio of 1:12. Later, 30 wt.% of beads catalyst was added to the PHM before the reaction started. Figure 10 showed a schematic image for the open-system reactor, which was used in this experiment.

The mixture of the product was separated by the centrifugation process to recover the spent catalyst. The final product was observed as three layers with the top layer containing biodiesel, the middle layer containing glycerol, and the bottom layer was the catalyst. For the beads catalyst, after the reaction ended, the catalyst was separated by removing PHM, followed by centrifugation process. As the top layer found was biodiesel, the biodiesel needs to wash up by hot water by using a separating funnel several time to remove impurities such as excess glycerol and methanol. After that, the biodiesel was transferred into the beaker and heated up at 100 °C for 2 to 5 min to remove excess water from the washing process. Finally, the biodiesel was collected for the determination of FAME yield using 7860B Agilent gas chromatography-mass spectroscopy (GC-MS). The injector and detector temperature were programmed at 240 °C. Helium was used as the carrier gas with a flow rate of 19.2 mL min⁻¹. The Agilent J&W (Selangor, Malaysia) column temperature was set at 150 °C with ramping rate 15 °C min⁻¹.

3.5. Determination of Ester Content

Table 5 shows the formula to calculate the biodiesel from the conversion until the pure result, and Equation (1) shows the classical technique to calculate biodiesel where A refers to the mass of the product obtained divided by the mass of the WCO [62]. However, due to the presence of impurities stated in Section 2.5, this formula cannot reflect the true estimate of the collected biodiesel [63]. Hence, Equations (2)–(4) suggested the most accurate formula to determine the exact amount of FAME in the product.

Table 5. Equations to calculate the biodiesel conversion, ester content, and biodiesel yield.

Formula	Equation	Nr.
Conversion (%) *	$d = \frac{A}{\text{Mass of WCO}} \times 100\%$	(1)
Ester content (%) From EN 14103	$c = \frac{TA-AEI}{AEI} \times \frac{CEI \times VEI}{m} \times 100$	(2)
Mass of pure biodiesel from biodiesel conversion (g)	$Y = c \times A$	(3)
Pure biodiesel yield (%)	$\text{FAME yield, \%} = \frac{Y \text{ (g)}}{\text{mass WCO (g)}} \times 100\%$	(4)

* Conventional technique to estimate the biodiesel conversion.

Therefore, to obtain the actual mass of the pure biodiesel, the GC peaks area of FAME present in the product was determined by adding the internal standard of methyl heptadecanoate and comparing with the biodiesel standard. Thus, the FAME yield or percentage of ester content was determined based on Equations (2)–(4) as indicated by Agilent standard method EN14103. Where c refers to the ester content in biodiesel sample, TA for the total area, AEI for the area of internal standard, CEI for the concentration (mg mL⁻¹) of methyl heptadecanoate solution, VEI for the volume (mL) of methyl heptadecanoate solution, and m for the mass of the sample.

4. Conclusions

K₂CO₃ and KOH supported onto Al₂O₃ beads and powder successfully converted a waste cooking oil to biodiesel via transesterification process. With an optimum reaction condition of catalyst concentration of 30%, oil to methanol ratio of 1:12, catalyst loading of 5 wt%, and reaction temperature of 65 °C, the following yields of pure biodiesel were obtained: 86.8% for beads KOH/Al₂O₃ catalyst at 2 h reaction time, 77.4% for beads K₂CO₃/Al₂O₃ catalyst at 2 h, 66.7% for powder KOH/Al₂O₃ catalyst at 3 h, and 72.3% for powder K₂CO₃/Al₂O₃ catalyst at 4 h. In terms of biodiesel yield, KOH/Al₂O₃ catalyst shows the highest biodiesel yield collected, but K₂CO₃/Al₂O₃ catalyst offers better reusability (up to 6 times for K₂CO₃/Al₂O₃ powder catalyst and 7 times for K₂CO₃/Al₂O₃ beads catalyst) by using PHM as the reactor container. Based on the result, in between powder and beads catalysts, beads catalyst can be considered a better alternative to powder heterogeneous and normal homogeneous catalyst for biodiesel production as it can be easily recovered, can be reuse back without mass loss of the catalyst, and proved suitable for an industrial-scale application. Overall, beads K₂CO₃/Al₂O₃ catalyst shows better performance and PHM was suitable as the reaction container in the transesterification process, as it maintains the original shape and mass of beads catalyst.

Author Contributions: Writing—original draft preparation, M.A.H.L.N.; conceptualization, M.A.H.L.N.; methodology, M.A.H.L.N. and R.F.A.; writing—review and editing, N.A.M.S., W.N.A.W.M. and M.L.I.; validation, R.F.A., N.A.M.S., W.N.A.W.M. and M.L.I.; supervision, N.A.M.S., W.N.A.W.M. and M.L.I. All authors have read and agreed to the published version of the manuscript.

Funding: This research was funded by Malaysia Higher Education for the FRGS research fund File No. 600 IRMI/FRGS 5/3(108/2019).

Institutional Review Board Statement: Not applicable.

Informed Consent Statement: Not applicable.

Data Availability Statement: All data is contained within the article.

Acknowledgments: The authors acknowledged the funding from Research Grant, FRGS with Grant No.: 011000190001 (File no.: 600 IRMI/FRGS 5/3(108/2019)). Special thanks to Gaanty Pragas Maniam from UMP, Asikin Mijan from UKM and Zul Adlan Mohd Hir from UiTM for his advice throughout the completion of this manuscript.

Conflicts of Interest: The authors declare no conflict of interest.

References

1. Sadaf, S.; Iqbal, J.; Ullah, I.; Bhatti, H.N.; Nouren, S.; Nisar, J.; Iqbal, M. Biodiesel production from waste cooking oil: An efficient technique to convert waste into biodiesel. *Sustain. Cities Soc.* **2018**, *41*, 220–226. [[CrossRef](#)]
2. Trejda, M.; Nurwita, A.; Kryszak, D. Synthesis of solid acid catalysts for esterification with the assistance of elevated pressure. *Microporous Mesoporous Mater.* **2019**, *278*, 115–120. [[CrossRef](#)]
3. Ganesan, S.; Arunkumar, T.; Munuswamy, D.; Appavu, P.; Devarajan, Y. Effect of egr & nanoparticles on performance and emission characteristics of a diesel engine fuelled with palm biodiesel and diesel blends. *J. Oil Palm. Res.* **2019**, *31*, 130–137. [[CrossRef](#)]
4. Mohd Shohaimi, N.A.; Wan Abu Bakar, W.A.; Jaafar, J. The catalytic deacidification of acidic crude oil using Cu-doped alkaline earth metal oxide catalysts. *Pet. Sci. Technol.* **2017**, *35*, 1097–1103. [[CrossRef](#)]
5. Mohadesi, M.; Aghel, B.; Maleki, M.; Ansari, A. The use of KOH/Clinoptilolite catalyst in pilot of microreactor for biodiesel production from waste cooking oil. *Fuel* **2019**, 116659. [[CrossRef](#)]
6. Lokman, I.M.; Rashid, U.; Taufiq-Yap, Y.H.; Yunus, R. Methyl ester production from palm fatty acid distillate using sulfonated glucose-derived acid catalyst. *Renew. Energy* **2015**, *81*, 347–354. [[CrossRef](#)]
7. Liu, F.; Ma, X.; Li, H.; Wang, Y.; Cui, P.; Guo, M.; Yaxin, H.; Lu, W.; Zhou, S.; Yu, M. Dilute sulfonic acid post functionalized metal organic framework as a heterogeneous acid catalyst for esterification to produce biodiesel. *Fuel* **2020**, *266*, 117149. [[CrossRef](#)]
8. Khodamorady, M.; Sohrabnezhad, S.; Bahrami, K. Efficient one-pot synthetic methods for the preparation of 3,4-dihydropyrimidinones and 1,4-dihydropyridine derivatives using BNPs@SiO₂(CH₂)₃NH₂SO₃H as a ligand and metal free acidic heterogeneous nano-catalyst. *Polyhedron* **2020**, *178*, 114340. [[CrossRef](#)]
9. Noiroj, K.; Intarapong, P.; Luengnaruemitchai, A.; Jai-In, S. A comparative study of KOH/Al₂O₃ and KOH/NaY catalysts for biodiesel production via transesterification from palm oil. *Renew. Energy* **2009**, *34*, 1145–1150. [[CrossRef](#)]

10. Shohaimi, N.A.M.; Wan Abu Bakar, W.A.; Jaafar, J. Catalytic neutralization method for naphthenic acid removal in crude oil by alumina supported Ca and Ba catalysts. *Pet. Sci. Technol.* **2014**, *32*, 2365–2375. [[CrossRef](#)]
11. Du, L.; Li, Z.; Ding, S.; Chen, C.; Qu, S.; Yi, W.; Lu, J.; Ding, J. Synthesis and characterization of carbon-based MgO catalysts for biodiesel production from castor oil. *Fuel* **2019**, *258*, 116122. [[CrossRef](#)]
12. Ahmad Farid, M.A.; Hassan, M.A.; Taufiq-Yap, Y.H.; Ibrahim, M.L.; Hasan, M.Y.; Ali, A.A.M.; Othman, M.R.; Shirai, Y. Kinetic and thermodynamic of heterogeneously K_3PO_4/AC -catalysed transesterification via pseudo-first order mechanism and Eyring-Polanyi equation. *Fuel* **2018**, *232*, 653–658. [[CrossRef](#)]
13. Hazmi, B.; Rashid, U.; Taufiq-yap, Y.H.; Ibrahim, M.L. Supermagnetic nano-bifunctional catalyst from rice husk: Synthesis, characterization and application for conversion of used cooking oil to biodiesel. *Catalysts* **2020**, *10*, 225. [[CrossRef](#)]
14. Nayezbadeh, H.; Saghatoleslami, N.; Tabasizadeh, M. Optimization of the activity of KOH/calcium aluminate nanocatalyst for biodiesel production using response surface methodology. *J. Taiwan Inst. Chem. Eng.* **2016**, *68*, 379–386. [[CrossRef](#)]
15. Lam, M.K.; Lee, K.T.; Mohamed, A.R. Homogeneous, heterogeneous and enzymatic catalysis for transesterification of high free fatty acid oil (waste cooking oil) to biodiesel: A review. *Biotechnol. Adv.* **2010**, *28*, 500–518. [[CrossRef](#)] [[PubMed](#)]
16. Tangy, A.; Pulidindi, I.N.; Perkas, N.; Gedanken, A. Continuous flow through a microwave oven for the large-scale production of biodiesel from waste cooking oil. *Bioresour. Technol.* **2017**, *224*, 333–341. [[CrossRef](#)]
17. Nomanbhay, S.; Ong, M.Y. A review of microwave-assisted reactions for biodiesel production. *Bioengineering* **2017**, *4*, 57. [[CrossRef](#)]
18. Silveira Junior, E.G.; Perez, V.H.; Reyer, I.; Serrano-Lotina, A.; Justo, O.R. Biodiesel production from heterogeneous catalysts based K_2CO_3 supported on extruded $\Gamma-Al_2O_3$. *Fuel* **2019**, *241*, 311–318. [[CrossRef](#)]
19. Da Costa Evangelista, J.P.; Gondim, A.D.; Souza, L.D.; Araujo, A.S. Alumina-supported potassium compounds as heterogeneous catalysts for biodiesel production: A review. *Renew. Sustain. Energy Rev.* **2016**, *59*, 887–894. [[CrossRef](#)]
20. Zhu, M.; Li, B.; Jehng, J.M.; Sharma, L.; Taborda, J.; Zhang, L.; Stach, E.; Wachs, I.E.; Wu, Z.; Baltrusaitis, J. Molecular structure and sour gas surface chemistry of supported $K_2O/WO_3/Al_2O_3$ catalysts. *Appl. Catal. B Environ.* **2018**, *232*, 146–154. [[CrossRef](#)]
21. Ilgen, O.; Akin, A.N. Development of alumina supported alkaline catalysts used for biodiesel production. *Turkish J. Chem.* **2009**, *33*, 281–287. [[CrossRef](#)]
22. Ma, G.; Hu, W.; Pei, H.; Jiang, L.; Ji, Y.; Mu, R. Study of KOH/ Al_2O_3 as heterogeneous catalyst for biodiesel production via in situ transesterification from microalgae. *Environ. Technol.* **2015**, *36*, 622–627. [[CrossRef](#)] [[PubMed](#)]
23. Lee, K.B.; Verdooren, A.; Caram, H.S.; Sircar, S. Chemisorption of carbon dioxide on potassium-carbonate-promoted hydrotalcite. *J. Colloid Interface Sci.* **2007**, *308*, 30–39. [[CrossRef](#)] [[PubMed](#)]
24. Schaefer, S.; Fierro, V.; Szczurek, A.; Izquierdo, M.T.; Celzard, A. Physisorption, chemisorption and spill-over contributions to hydrogen storage. *Int. J. Hydrogen Energy* **2016**, *41*, 17442–17452. [[CrossRef](#)]
25. Abdullah, A.; Rahmawati Sianipar, R.N.; Ariyani, D.; Nata, I.F. Conversion of palm oil sludge to biodiesel using alum and KOH as catalysts. *Sustain. Environ. Res.* **2017**, *27*, 291–295. [[CrossRef](#)]
26. Boonprasop, S.; Chalermssinsuwan, B.; Piumsomboon, P. Effect of operating parameters of potassium carbonate supported on gamma alumina ($K_2CO_3/\gamma-Al_2O_3$) on CO_2 capture capacity using depressurized regeneration. *J. Taiwan Inst. Chem. Eng.* **2018**, *88*, 215–225. [[CrossRef](#)]
27. Postole, G.; Nguyen, T.S.; Aouine, M.; Gélín, P.; Cardenas, L.; Piccolo, L. Efficient hydrogen production from methane over iridium-doped ceria catalysts synthesized by solution combustion. *Appl. Catal. B Environ.* **2015**, *166–167*, 580–591. [[CrossRef](#)]
28. Veselovskaya, J.V.; Derevschikov, V.S.; Kardash, T.Y.; Stonkus, O.A.; Trubitsina, T.A.; Okunev, A.G. Direct CO_2 capture from ambient air using K_2CO_3/Al_2O_3 composite sorbent. *Int. J. Greenh. Gas. Control.* **2013**, *17*, 332–340. [[CrossRef](#)]
29. Silveira, E.G.; Barcelos, L.F.T.; Perez, V.H.; Justo, O.R.; Ramirez, L.C.; Rêgo Filho, L.; de Castro, M.P.P. Biodiesel production from non-edible forage turnip oil by extruded catalyst. *Ind. Crops Prod.* **2019**, *139*, 111503. [[CrossRef](#)]
30. Sharikh, A.M.; Sulaiman, S.; Azmi, A.S.; Sulaiman, S.Z. Potassium carbonate from pineapple and orange peels as catalyst for biodiesel production. *AIP Conf. Proc.* **2018**, *2030*, 020290. [[CrossRef](#)]
31. Malins, K. The potential of K_3PO_4 , K_2CO_3 , Na_3PO_4 and Na_2CO_3 as reusable alkaline catalysts for practical application in biodiesel production. *Fuel Process. Technol.* **2018**, *179*, 302–312. [[CrossRef](#)]
32. Ruhul, A.M.; Kalam, M.A.; Masjuki, H.H.; Fattah, I.M.R.; Reham, S.S.; Rashed, M.M. State of the art of biodiesel production processes: A review of the heterogeneous catalyst. *RSC Adv.* **2015**, *5*, 101023–101044. [[CrossRef](#)]
33. Mohamed, M.A.; Wan Salleh, W.N.; Jaafar, J.; Rosmi, M.S.; Zul, Z.A.; Abd Mutalib, M.; Ismail, A.F.; Tanemura, M. Carbon as amorphous shell and interstitial dopant in mesoporous rutile TiO_2 : Bio-Template assisted sol-gel synthesis and photocatalytic activity. *Appl. Surf. Sci.* **2017**, *393*, 46–59. [[CrossRef](#)]
34. Islam, A.; Taufiq-Yap, Y.H.; Ravindra, P.; Teo, S.H.; Sivasangar, S.; Chan, E.S. Biodiesel synthesis over millimetric $\gamma-Al_2O_3/KI$ catalyst. *Energy* **2015**, *89*, 965–973. [[CrossRef](#)]
35. Raj, K.J.A.; Ramaswamy, A.V.; Viswanathan, B. Surface area, pore size, and particle size engineering of titania with seeding technique and phosphate modification. *J. Phys. Chem. C* **2009**, *113*, 13750–13757. [[CrossRef](#)]
36. Mohd Hir, Z.A.; Abdullah, A.H.; Zainal, Z.; Lim, H.N. Visible light-active hybrid film photocatalyst of polyethersulfone-reduced TiO_2 : Photocatalytic response and radical trapping investigation. *J. Mater. Sci.* **2018**, *53*, 13264–13279. [[CrossRef](#)]
37. Shan, R.; Shi, J.; Yan, B.; Chen, G.; Yao, J.; Liu, C. Transesterification of palm oil to fatty acids methyl ester using K_2CO_3 /palygorskite catalyst. *Energy Convers. Manag.* **2016**, *116*, 142–149. [[CrossRef](#)]

38. Ibrahim, M.L.; Nik Abdul Khalil, N.N.A.; Islam, A.; Rashid, U.; Ibrahim, S.F.; Sinar Mashuri, S.I.; Taufiq-Yap, Y.H. Preparation of Na₂O supported CNTs nanocatalyst for efficient biodiesel production from waste-oil. *Energy Convers. Manag.* **2020**, *205*, 112445. [[CrossRef](#)]
39. Smyrnioti, M.; Tampaxis, C.; Steriotis, T.; Ioannides, T. Study of CO₂ adsorption on a commercial CuO/ZnO/Al₂O₃ catalyst. *Catal. Today* **2020**, *357*, 495–502. [[CrossRef](#)]
40. Rahmani Vahid, B.; Haghighi, M.; Alaei, S.; Toghiani, J. Reusability enhancement of combustion synthesized MgO/MgAl₂O₄ nanocatalyst in biodiesel production by glow discharge plasma treatment. *Energy Convers. Manag.* **2017**, *143*, 23–32. [[CrossRef](#)]
41. Ahmad Farid, M.A.; Hassan, M.A.; Taufiq-Yap, Y.H.; Ibrahim, M.L.; Othman, M.R.; Ali, A.A.M.; Shirai, Y. Production of methyl esters from waste cooking oil using a heterogeneous biomass-based catalyst. *Renew. Energy* **2017**, *114*, 638–643. [[CrossRef](#)]
42. Lokman Nohakim, M.A.H.; Mohd Shohaimi, N.A.; Ibrahim, M.L.; Wan Mokhtar, W.N.A.; Abdul Halim, A.Z. Transesterification of waste cooking oil utilizing heterogeneous K₂CO₃/Al₂O₃ and KOH/Al₂O₃ catalysts. *Malays. Inst. Chem.* **2021**, *23*, 74–83.
43. Hong, Y.; Wu, G. Heterogeneous and efficient transesterification of *Jatropha curcas* L. seed oil to produce biodiesel catalysed by nano-sized SO₄²⁻/TiO₂. *R. Soc. Open Sci.* **2018**, *5*, 181331.
44. Alonso, D.M.; Mariscal, R.; Moreno-Tost, R.; Poves, M.D.Z.; Granados, M.L. Potassium leaching during triglyceride transesterification using K/γ-Al₂O₃ catalysts. *Catal. Commun.* **2007**, *8*, 2074–2080. [[CrossRef](#)]
45. Astuti, W.; Prilitasari, N.M.; Iskandar, Y.; Bratakusuma, D.; Petrus, H.T.B.M. Leaching behavior of lanthanum, nickel and iron from spent catalyst using inorganic acids. *IOP Conf. Ser. Mater. Sci. Eng.* **2018**, *285*, 012007. [[CrossRef](#)]
46. Saba, T.; Estephane, J.; El Khoury, B.; El Khoury, M.; Khazma, M.; El Zakhem, H.; Aouad, S. Biodiesel production from refined sunflower vegetable oil over KOH/ZSM5 catalysts. *Renew. Energy* **2016**, *90*, 301–306. [[CrossRef](#)]
47. Ngamcharussrivichai, C.; Wiwatnimit, W.; Wangnoi, S. Modified dolomites as catalysts for palm kernel oil transesterification. *J. Mol. Catal. A Chem.* **2007**, *276*, 24–33. [[CrossRef](#)]
48. Ngamcharussrivichai, C.; Nunthasanti, P.; Tanachai, S.; Bunyakiat, K. Biodiesel production through transesterification over natural calciums. *Fuel Process. Technol.* **2010**, *91*, 1409–1415. [[CrossRef](#)]
49. Kang, S.; Li, X.; Fan, J.; Chang, J. Characterization of hydrochars produced by hydrothermal carbonization of lignin, cellulose, d-xylose, and wood meal. *Ind. Eng. Chem. Res.* **2012**, *51*, 9023–9031. [[CrossRef](#)]
50. Pasupulety, N.; Gunda, K.; Liu, Y.; Rempel, G.L.; Ng, F.T.T. Production of biodiesel from soybean oil on CaO/Al₂O₃ solid base catalysts. *Appl. Catal. A Gen.* **2013**, *452*, 189–202. [[CrossRef](#)]
51. Borah, M.J.; Devi, A.; Saikia, R.A.; Deka, D. Biodiesel production from waste cooking oil catalyzed by in-situ decorated TiO₂ on reduced graphene oxide nanocomposite. *Energy* **2018**, *158*, 881–889. [[CrossRef](#)]
52. Fadzilah, R.; Rashid, U.; Lokman, M.; Hazmi, B.; Alharthi, A.; Arbi, I. Bifunctional nano-catalyst produced from palm kernel shell via hydrothermal-assisted carbonization for biodiesel production from waste cooking oil. *Renew. Sustain. Energy Rev.* **2021**, *137*, 110638. [[CrossRef](#)]
53. Kalderis, D.; Kotti, M.S.; Méndez, A.; Gascó, G. Characterization of hydrochars produced by hydrothermal carbonization of rice husk. *Solid Earth* **2014**, *5*, 477–483. [[CrossRef](#)]
54. Abdullah, R.F.; Rashid, U.; Tau, H. Synthesis of bifunctional nanocatalyst from waste palm kernel shell and its application for biodiesel production. *RSC Adv.* **2020**, *4*, 27183–27193. [[CrossRef](#)]
55. Mohd Hir, Z.A.; Abdullah, A.H.; Zainal, Z.; Lim, H.N. Photoactive hybrid photocatalyst of polyethersulfone-zno for the degradation of methyl orange dye: Kinetic study and operational parameters. *Catalyst* **2017**, *17*, 313. [[CrossRef](#)]
56. Boz, N.; Degirmenbasi, N.; Kalyon, D.M. Transesterification of canola oil to biodiesel using calcium bentonite functionalized with K compounds. *Appl. Catal. B Environ.* **2013**, *138*, 236–242. [[CrossRef](#)]
57. Rajkhowa, T.; Marin, G.B.; Thybaut, J.W. Quantifying the dominant factors in Cu catalyst deactivation during glycerol hydrogenolysis. *J. Ind. Eng. Chem.* **2017**, *54*, 270–277. [[CrossRef](#)]
58. Ning, X.; Zhan, L.; Wang, H.; Yu, H.; Peng, F. Deactivation and regeneration of: In situ formed bismuth-promoted platinum catalyst for the selective oxidation of glycerol to dihydroxyacetone. *New J. Chem.* **2018**, *42*, 18837–18843. [[CrossRef](#)]
59. Yori, J.C.; D’Ippolito, S.A.; Pieck, C.L.; Vera, C.R. Deglycerolization of biodiesel streams by adsorption over silica beds. *Energy Fuels* **2007**, *21*, 347–353. [[CrossRef](#)]
60. Delmon, B.; Haber, J.; Block, J.H. Manual of methods and procedures for catalyst characterization (technical report). *Pure Appl. Chem.* **1995**, *67*, 1257–1306. [[CrossRef](#)]
61. Yaşar, F. Biodiesel production via waste eggshell as a low-cost heterogeneous catalyst: Its effects on some critical fuel properties and comparison with CaO. *Fuel* **2019**, *255*, 115828. [[CrossRef](#)]
62. Vargas, E.M.; Neves, M.C.; Tarelho, L.A.C.; Nunes, M.I. Solid catalysts obtained from wastes for FAME production using mixtures of refined palm oil and waste cooking oils. *Renew. Energy* **2019**, *136*, 873–883. [[CrossRef](#)]
63. Labib, T.M.; Hawash, S.I.; El-Khatib, K.M.; Sharaky, A.M.; El Diwani, G.I.; Abdel Kader, E. Kinetic study and techno-economic indicators for base catalyzed transesterification of *Jatropha* oil. *Egypt. J. Pet.* **2013**, *22*, 9–16. [[CrossRef](#)]